

THE OFFICIAL MAGAZINE OF THE OCEANOGRAPHY SOCIETY

# Oceanography

## CITATION

Shroyer, E.L., D.L. Rudnick, J.T. Farrar, B. Lim, S.K. Venayagamoorthy, L.C. St. Laurent, A. Garanaik, and J.N. Moum. 2016. Modification of upper-ocean temperature structure by subsurface mixing in the presence of strong salinity stratification. *Oceanography* 29(2):62–71, <http://dx.doi.org/10.5670/oceanog.2016.39>.

## DOI

<http://dx.doi.org/10.5670/oceanog.2016.39>

## COPYRIGHT

This article has been published in *Oceanography*, Volume 29, Number 2, a quarterly journal of The Oceanography Society. Copyright 2016 by The Oceanography Society. All rights reserved.

## USAGE

Permission is granted to copy this article for use in teaching and research. Republication, systematic reproduction, or collective redistribution of any portion of this article by photocopy machine, reposting, or other means is permitted only with the approval of The Oceanography Society. Send all correspondence to: [info@tos.org](mailto:info@tos.org) or The Oceanography Society, PO Box 1931, Rockville, MD 20849-1931, USA.

# Modification of Upper-Ocean Temperature Structure by Subsurface Mixing in the Presence of Strong Salinity Stratification

By Emily L. Shroyer, Daniel L. Rudnick, J. Thomas Farrar, Byungho Lim, S. Karan Venayagamoorthy, Louis C. St. Laurent, Amrapalli Garankalk, and James N. Moum

Photo credit: San Nguyen

**ABSTRACT.** The Bay of Bengal has a complex upper-ocean temperature and salinity structure that is, in places, characterized by strong salinity stratification and multiple inversions in temperature. Here, two short time series from continuously profiling floats, equipped with microstructure sensors to measure subsurface mixing, are used to highlight implications of complex hydrography on upper-ocean heat content and the evolution of sea surface temperature. Weak mixing coupled with the existence of subsurface warm layers suggest the potential for storage of heat below the surface mixed layer over relatively long time scales. On the diurnal time scale, these data demonstrate the competing effects of surface heat flux and subsurface mixing in the presence of thin salinity-stratified mixed layers with temperature inversions. Pre-existing stratification can amplify the sea surface temperature response through control on the vertical extent of heating and cooling by surface fluxes. In contrast, subsurface mixing entrains relatively cool water during the day and relatively warm water during the night, damping the response to daytime heating and nighttime cooling at the surface. These observations hint at the challenges involved in improving monsoon prediction at longer, intraseasonal time scales as models may need to resolve upper-ocean variability over short time and fine vertical scales.

## INTRODUCTION

Two defining features of the Bay of Bengal (BoB) are its low near-surface salinity and strong monsoon forcing (Schott and McCreary, 2001; Rao and Sivakumar, 2003). These two components are related and depend on one another. Freshwater is added to the BoB through heavy precipitation and terrestrial runoff that accompany

the monsoon. The resultant strongly stratified upper ocean, in which salinity is regularly the dominant contributor to density (Agarwal et al., 2012), supports a complex upper-ocean temperature structure with direct consequences for sea surface temperature (SST). In turn, oceanic control on the upper-ocean hydrographic structure can alter SST, influencing

air-sea exchange of heat and freshwater and thereby creating a feedback pathway between the atmosphere and ocean (Fu et al., 2003; Woolnough et al., 2007; Guemas et al., 2011; McPhaden and Foltz, 2013). Consequently, understanding the diversity of the processes that set upper-ocean stratification and SST in the BoB is important for improving monsoon prediction (Inness and Slingo, 2003; Bernie et al., 2005; Woolnough et al., 2007; Sobel et al., 2008), particularly on intraseasonal time scales over which current forecast capabilities are poor (Goswami et al., 2006, 2011). Further discussion of the region and its significance in the South Asian monsoon can be found in Goswami et al. (2016, in this issue).

On seasonal time scales, monsoon forcing and the lateral spreading of freshwater from multiple terrestrial sources regulate mixed layer depth and SST (Rao and Sivakumar, 2003; Sengupta et al., 2006; Vinayachandran and Nanjundiah, 2009). During the northeast monsoon (boreal winter), winds from the northeast carry dry air from the Indian

subcontinent over the Bay of Bengal, where it accumulates moisture and then causes heavy rainfall over southern India and northeast Sri Lanka. During the southwest monsoon (boreal summer), winds from the southwest carry moisture-laden air toward the Himalayas, resulting in heavy rainfall over the Bay of Bengal's northern rim nations, feeding the Ganges-Brahmaputra and Irrawaddy watersheds. Although much of the terrestrial runoff is carried in boundary currents around the BoB, the freshwater signature from northern rivers is observed annually in the interior of the BoB in late summer (M. Ravichandran, Indian National Centre for Ocean Information Services, *pers. comm.*, May 2015). Beginning at this time and continuing through early spring, the salinity stratification in the interior BoB rivals that of temperature stratification in setting the upper-ocean density field. A salinity-stratified mixed layer allows for inversions in upper-ocean temperature profiles and the creation of a barrier layer (Agarwal et al., 2012), defined as the region between the mixed layer and the thermocline (Mignot et al., 2009). The barrier layer isolates cool thermocline water from the surface mixed layer (Lukas and Lindstrom, 1991).

Resolving upper-ocean variability at time scales as short as the diurnal can have important consequences for SST evolution on longer time scales, including intraseasonal variability (Bernie et al., 2005; Guemas et al., 2011; Mujumdar et al., 2011). Intraseasonal variability in the southwest monsoon is marked by active periods with heavy cloud cover and precipitation and break periods with little to no precipitation. During cloud-free break periods, strong insolation leads to the development of a diurnal warm layer (DWL) within the ocean mixed layer. The depth to which this heat penetrates determines the amplitude of the daily SST cycle within the DWL, with deeper penetration resulting in a weaker SST cycle (Fairall et al., 1996). During active periods of the monsoon, the short-wave radiation (sunlight) is reduced by heavy cloud cover and may remain negligible for several days at a time in comparison to the sensible, latent, and longwave components (Sengupta et al., 2001; Sobel et al., 2008). Under these conditions, air-sea fluxes act to cool the ocean's surface, limiting formation of a DWL. Because of the complexity of the upper-ocean temperature structure, subsurface mixing (see Science Box 1) may also alternately cool and heat the sea surface, complicating the response of the DWL to surface fluxes.

## SCIENCE BOX 1. TURBULENCE → MICROSTRUCTURE → MIXING

The discussion in this paper of the contribution of mixing to modulation of the diurnal warm layer relates to processes beneath the air-sea interface—hence, we refer here to this contribution as **subsurface mixing**. Mixing is an irreversible thermodynamic process by which scalar properties (like heat) diffuse at molecular scales. According to Fick's Law, the molecular diffusive flux of a scalar  $\Phi$  is  $-\gamma \partial \Phi / \partial x_j$ , where  $\gamma$  is the molecular diffusivity and  $\partial \Phi / \partial x_j$  is the mean scalar gradient. The negative sign indicates that molecular diffusion is always a down-gradient process, moving properties from regions of high concentration to regions of low concentration. The  $\gamma$  term is a property of the fluid that is measurable under laboratory conditions and varies weakly with temperature, pressure, and salinity. In the ocean, the molecular diffusivity of heat varies by around 15%, ranging from  $\gamma_T = 1.36 \times 10^{-7} \text{ m}^2 \text{ s}^{-1}$  for fresh, cool water (0 gm kg<sup>-1</sup>, 0°C) to  $\gamma_T = 1.51 \times 10^{-7} \text{ m}^2 \text{ s}^{-1}$  for warm, salty water (40 gm kg<sup>-1</sup>, 30°C).

Fluid dynamic instabilities (e.g., shear instability and convection) lead to fully three-dimensional **turbulence**, a consequence of which is scalar **microstructure**, small-scale eddies and overturns that enhance scalar gradients in all three dimensions as depicted in the lower right-hand corner of Figure SB1. Sensors to measure ocean microstructure, like the fast thermistors on the  $\chi$ SOLOs discussed here, provide a measure of these enhanced gradients. These small-scale gradients can be many orders of magnitude greater than mean background vertical gradients, consequently leading to enhanced molecular mixing that is several orders of magnitude greater than predicted by Fick's law.

We often model the effect of turbulence on mixing in the ocean using a turbulence diffusivity, which is a property of the fluid flow and varies in space and time. The diffusive term in the heat equation is thus modeled as a combination of turbulent and molecular diffusivities,  $\partial / \partial x_j \{ \rho c_p (K_T + \gamma_T) \partial T / \partial x_j \}$ , where  $\rho$  is the density of seawater,  $c_p$  is the heat capacity of seawater, and  $K_T$  is the turbulent diffusivity of heat.  $K_T$ , a property of the flow, is inferred from measurements of the ocean's microstructure. Unlike molecular diffusivity, turbulence diffusivity varies widely, as shown in the  $\chi$ SOLO data, in which  $K_T$  ranges by five orders of magnitude from the molecular value to  $10^{-2} \text{ m}^2 \text{ s}^{-1}$ .

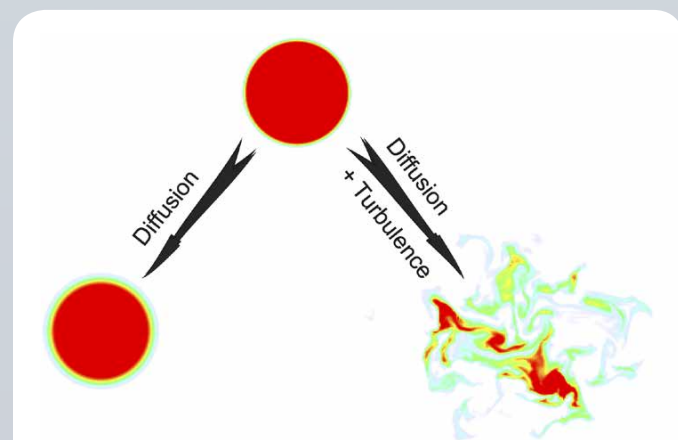


**FIGURE SB1.** A comparison of mixing enhanced by turbulence with mixing due to molecular processes alone, as revealed by a numerical solution of the equations of fluid motion. The initial state (top) includes a circular region of dyed fluid in a white background. Two possible evolutions are shown: one in which the fluid is motionless (save for random molecular motions) as shown on the bottom left, and one in which the fluid is in a state of fully developed turbulence (bottom right). The mixed region (yellow-green) diffuses much more rapidly in the turbulent case. From Smyth and Moum (2001)

Here, we detail upper-ocean structure in the northern BoB during the southwest monsoon using observations from two recent deployments of specialized profiling floats ( $\chi$ SOLO in Figure 1). These instruments combine the capabilities of the SOLO-II profiling float, which can be programmed to change its buoyancy and dive and rise on a schedule to sample conductivity-temperature-pressure at 1 Hz resolution (Roemmich et al., 2004), with  $\chi$ pod microstructure sensors to sample turbulent fluctuations at 100 Hz (Moum and Nash, 2009). The roughly week-long drifts followed along the periphery of a sea surface height low, which was mapped by satellite and indicates the presence of a geostrophic flow, centered near 17°N, 88°E. The signature of higher-frequency (primarily) tidal oscillations manifests as a wobble to the otherwise roughly geostrophic trajectories (Figure 1 inset). The northern  $\chi$ SOLO float (SN8382, referred to hereafter as

$\chi$ SOLO-N) generally sampled fresher water than the southern float (SN8371, referred to hereafter as  $\chi$ SOLO-S), consistent with the large-scale salinity gradients in the BoB (fresher water to the north). Both  $\chi$ SOLO floats were programmed to profile as rapidly as possible to ~50 m depth with ~25 minutes between successive profiles. The conductivity-temperature-pressure data were sent to shore through Iridium after each profile; higher-frequency microstructure data were stored internally in a self-contained unit. These data are used to demonstrate the complexity and variability of the upper-ocean temperature-salinity structure over daily to weekly time scales, with focus on the competing roles of net surface heat flux and subsurface mixing in the development of the DWL.

Although this work details a relatively coarse, bin-averaged (0.5 m vertical resolution) view of upper-ocean structure, we note that a primary strength of

the  $\chi$ SOLO technology lies in its ability to cleanly sample the upper ocean (see Science Box 2) and to resolve temperature within 1 cm of the ocean's surface. Since the  $\chi$ SOLO lacks a surface expression, it is decoupled from the surface, minimizing surface wave contamination relative to other platforms (e.g., buoy records). In addition, floats profile vertically relative to the water, allowing for straightforward conversion of frequency to wavenumber spectra (and consequently calculation of turbulence quantities), offering certain advantages over gliders and tethered profilers. This technology provides in situ high spatial (centimeters in the vertical) and high temporal (30 minutes for 50 m profiles) resolution that is capable of resolving the structure and evolution of the DWL and SST.

## UPPER-OCEAN SALINITY AND TEMPERATURE STRUCTURE

Atmospheric conditions varied from clear-sky strong solar heating to persistent cooling, as measured at the Woods Hole Oceanographic Institution (WHOI) air-sea buoy at 18°N, 89°E (Weller et al., 2016, in this issue).  $\chi$ SOLO-S, deployed on August 29, 2015, at 0700 IST (India Standard Time = UTC plus 5.5 hours), initially recorded a four-day period with a regular and strong diurnal cycle in net surface heat flux (Figure 2a) and relatively strong wind forcing (Figure 2b) before transitioning to a period of intermittent cooling and heating with generally light winds. The initial period of  $\chi$ SOLO-N (deployed September 2, 2015, 1900 IST) overlapped the second half of the  $\chi$ SOLO-S deployment. The latter part of the  $\chi$ SOLO-N drift was characterized by continuing light winds with most days experiencing diurnal heating (Figure 3a,b).

The complexity and variability of the upper-ocean temperature and salinity structure is evident through comparison of the two float time series (Figure 2c,d and Figure 3c,d). To the south, upper-ocean salinity was generally higher by 0.4 psu and temperature slightly warmer

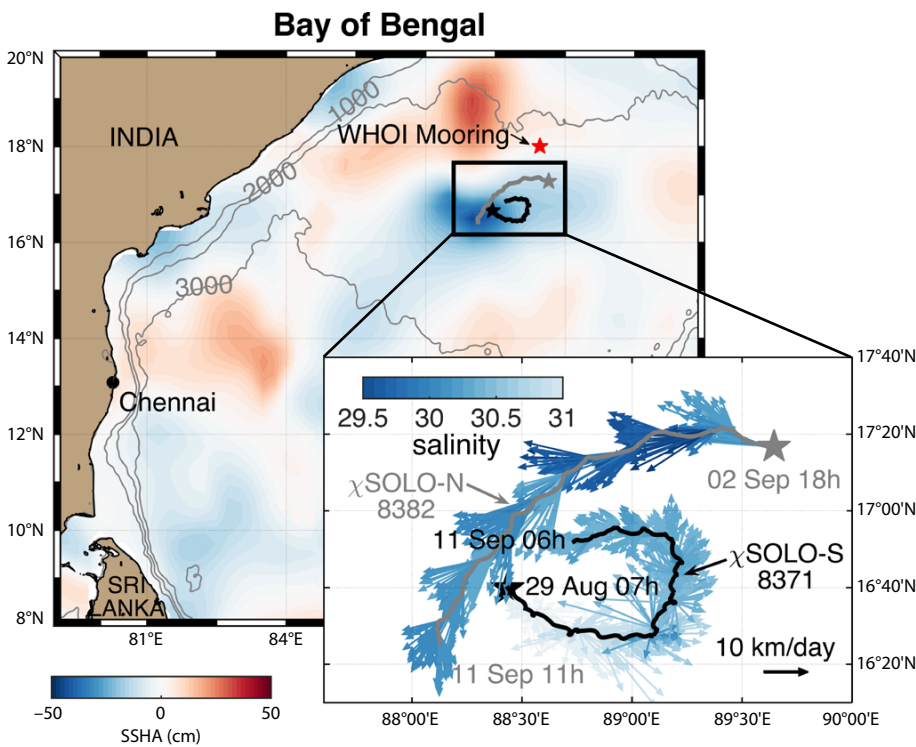


**FIGURE 1.** Background: Sea surface height anomaly (SSHA) with  $\chi$ SOLO trajectories (8371/ $\chi$ SOLO-S in black, 8382/ $\chi$ SOLO-N in gray). Stars indicate deployment locations. Isobaths are contoured in gray. Gridded SSHA data come from the Colorado Center for Astrodynamics Research (CCAR), available at <http://eddy.colorado.edu>. Inset: Salinity at 1 m (shading) and drift velocities (vectors). Start and end times are indicated. Times throughout the manuscript are in India Standard Time (IST, which is UTC plus 5.5 hours).

by 0.2°C compared to the northern float in the upper 15 m (density less than 1,019 kg m<sup>-3</sup>). Temperature and salinity were similar at depth (for water with potential density greater than 1,021.3 kg m<sup>-3</sup>), so that generally the salinity (density) stratification was greater to the north. Notably, almost the entire upper 50 m had temperature warmer than 28°C, a common threshold for atmospheric convection (Gadgil et al., 1984; Johnson and Xie, 2010).

The contribution of salinity to density stratification was typically more than 10 times greater than the destabilizing contribution from temperature at the base of the mixed layer (e.g., compare Figure 4b,c). The upper-ocean salinity stratification has multiple peaks, indicating the boundaries between stratified and well-mixed layers, while the temperature stratification regularly alternates sign, showing locations of temperature inversions. Qualitatively, the stratification for  $\chi$ SOLO-S is similar to that presented in Figure 4 for  $\chi$ SOLO-N, except that the stratification was slightly weaker. (Compare the spread of isopycnals plotted in Figures 2 and 3.) In both float records, stable temperature stratification develops near the surface on days with diurnal warming from insolation. The daytime heating is primarily constrained to within the pre-existing mixed layer. For example, the  $\chi$ SOLO-N record shows a very shallow DWL on day 1 that transitions to a much more diffuse, deeper feature on day 6 as the mixed layer deepens (Figure 4).

All profiles (total 1,077 profiles for the two floats combined) sampled at least one temperature inversion and often multiple inversions (Figures 2c,e; 3c,e; 4b,c). The uppermost inversion resides at the base of the salinity-controlled mixed layer (e.g., see Figure 4b,c for  $\chi$ SOLO-N). Subsurface maxima measured by the southern float were typically less than 0.4°C warmer than the surface. In contrast, subsurface warm layers were regularly more than 0.5°C warmer than the surface at the northern float. And, the subsurface maximum exceeded 0.9°C for a six-hour period spanning September 7–8.

As noted above, most of the sampled water column shows temperature greater than 28°C. Taking this as a reference temperature, an estimate of upper-ocean heat content (UOHC, J m<sup>-2</sup>) in excess of the threshold for atmospheric convection can be made using

$$\text{UOHC} = \sum_{>0} \rho_0 c_p (T - 28^\circ\text{C}) \times \Delta z,$$

where  $\rho_0$  is the reference density,  $c_p$  is the heat capacity of seawater,  $T$  is the measured temperature,  $\Delta z$  is the 0.5 m bin size of the gridded data, and the

## SCIENCE BOX 2. SURFACE WAVE CHARACTERIZATION WITH DIFFERENTIAL PRESSURE MEASUREMENTS

$\chi$ SOLO profiling through the sea surface provides a new perspective on near-surface (<5 m) properties and physics. In addition to thermistor data described in the main text,  $\chi$ SOLO floats also carried pitot tubes that provided high-resolution differential pressure measurements. Pitot measurements yielded several unique information streams (Figure SB2). First, the mean profiling speed of 0.18 m s<sup>-1</sup> can be determined directly from the pitot data. Second, the high-frequency signal (e.g., apparent between 18 m and 22 m depth in Figure SB2) denotes turbulent velocity fluctuations, which can be scaled to quantify the viscous rate of dissipation of the turbulence (Moum, 2015). A third and unique aspect of these near-surface profiles is the ability to characterize the surface wave field. In this example, the wave period (or frequency,  $\omega$ ) is directly estimated from the spectral peak in the profile, which occurs at four seconds in this example. The wavelength (or wavenumber,  $k$ ) is uniquely determined from the period for deepwater surface gravity waves. Finally, the vertical dependence is defined by the exponential decay and determines the wave amplitude  $\eta_0$  of 0.15 cm.

Future long profiling records such as this can contribute insight into the evolving surface wave field as well as the evolving structure of the diurnal warm layer and the mixed layer under a full range of conditions not accessible by ship.

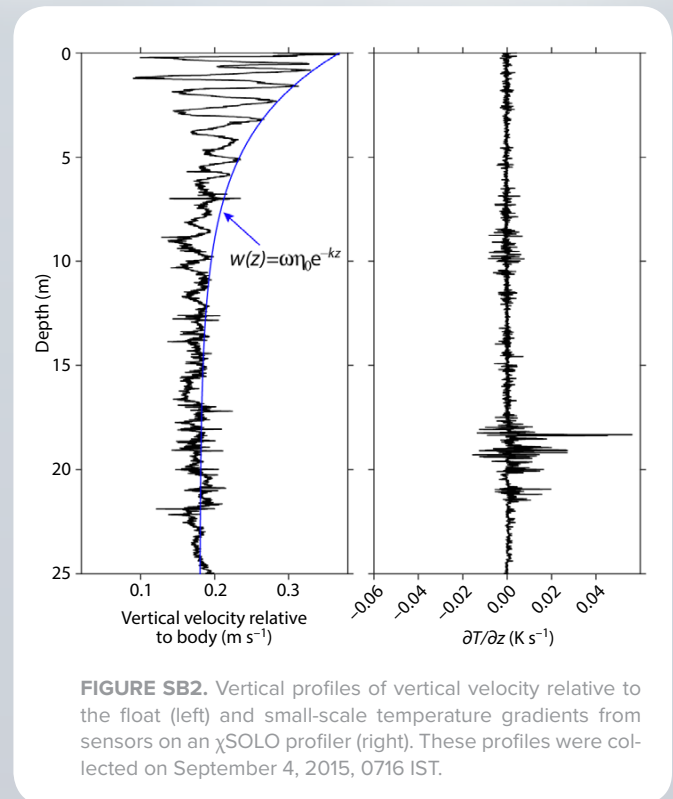


**FIGURE SB2.** Vertical profiles of vertical velocity relative to the float (left) and small-scale temperature gradients from sensors on a  $\chi$ SOLO profiler (right). These profiles were collected on September 4, 2015, 0716 IST.

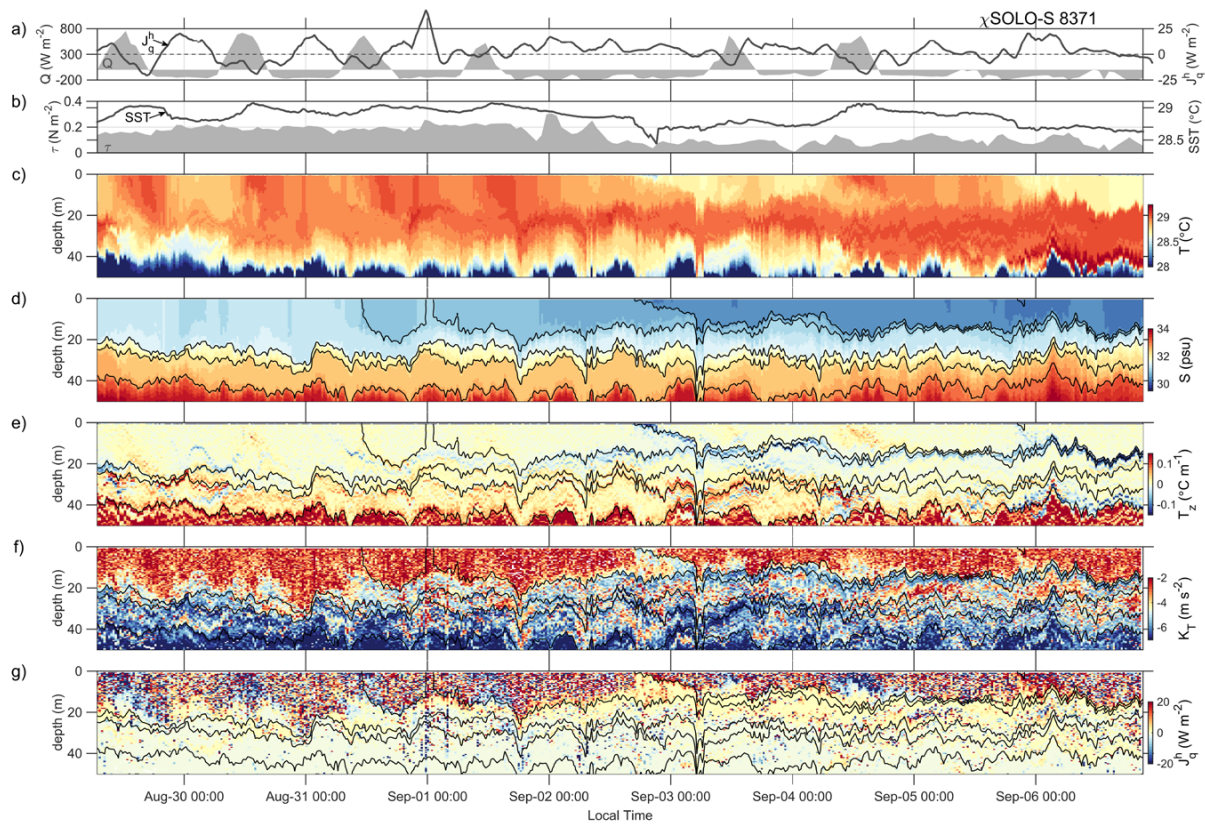


**FIGURE 2.** Summary of  $\chi$ SOLO-S. (a) Net surface heat flux from the Woods Hole Oceanographic Institution (WHOI) mooring at 18°N (shading, left-hand side) and turbulent heat flux averaged over the upper 10 m (black, right-hand side). (b) Wind stress from the WHOI mooring (shading, left-hand side) and sea surface temperature from the  $\chi$ SOLO (black, right-hand side). Time series show (c) temperature, (d) salinity, (e) vertical gradient of temperature, (f) turbulent diffusivity of temperature, and (g) turbulent heat flux. Positive turbulent heat flux corresponds to mixing of heat upward. Isopycnals are contoured in black at 0.25 kg m<sup>-3</sup> intervals in (c)–(g).

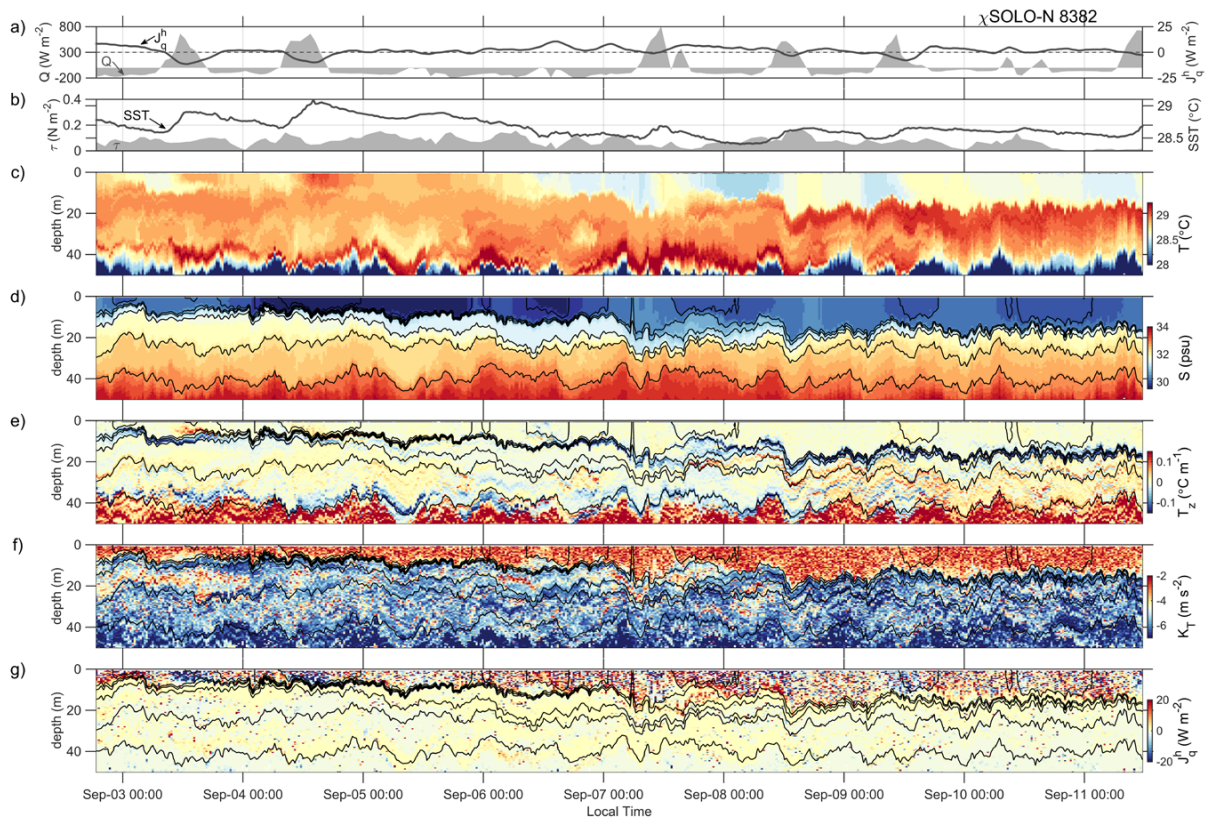


**FIGURE 3.** Summary of  $\chi$ SOLO-N—same as Figure 2.

summation includes only positive values. The average heat content per meter depth (in  $\text{J m}^{-3}$ ) within a layer of thickness,  $H$ , is given as  $H^{-1} \times \text{UOHC}$ , where the UOHC has been summed over the layer. We consider the average heat content within two separate layers in Figure 4a (right-hand side): above the mixed layer ( $H$  spans from the surface to the mixed layer depth) and below the mixed layer ( $H$  spans from the mixed layer depth to the depth where  $T = 28^\circ\text{C}$ ). We also convert UOHC to a daily rate using a set time scale,  $\Delta t = 1$  day, to convert  $\text{J m}^{-3}$  to the more familiar  $\text{W m}^{-2}$ . This conversion is made so that the heat contained in each depth bin can be compared to the heat gained or lost by the average net surface heat flux (Figure 4d).

The region between the surface mixed layer and  $\sim 50$  m depth typically contains  $>10 \text{ W m}^{-2}$  in each half-meter depth bin

(Figure 4d), that is, if a depth bin lost all of its heat relative to  $28^\circ\text{C}$  in one day, its heat flux would be  $>10 \text{ W m}^{-2}$ . The summed total  $\text{UOHC}/\Delta t$  is typically greater than  $1,800 \text{ W m}^{-2}$ . In other words, if cooling were capable of eroding salinity stratification near the surface, the UOHC is sufficient to maintain an SST of  $28^\circ\text{C}$  for roughly 10 days given daily average surface cooling of  $150\text{--}200 \text{ W m}^{-2}$  (i.e., conditions typical to those observed on days of net cooling during the  $\chi\text{SOLO}$  deployments). Furthermore, while the average heat content above the mixed layer depth responds to surface heat fluxes, the average heat content below the mixed layer is relatively uniform over the time series (Figure 4a, right-hand side). The response of the average heat content within the mixed layer to surface fluxes can be seen in the time rate of change of the dashed line in Figure 4a. For example,

its slope from days 2 to 4 corresponds to a cooling rate of roughly  $70 \text{ W m}^{-2}$ , consistent with the measured surface cooling at the WHOI mooring.

Due to the observed weak turbulent heat fluxes (as discussed in the following section), the UOHC has the potential to be stored for a long period of time once it is isolated below the surface mixed layer. Given the relatively weak net surface flux during the southwest monsoon (in the long-term, large-scale average long-wave and latent cooling roughly balance shortwave heating; Kalnay et al., 1996), warm layers could persist through this season. Periods of either sustained cooling (e.g., those accompanying the latent heat release associated with dry northeast monsoon winds) or intense wind forcing (e.g., those realized during storms or cyclones) will be needed in order to erode the subsurface maxima in temperature.

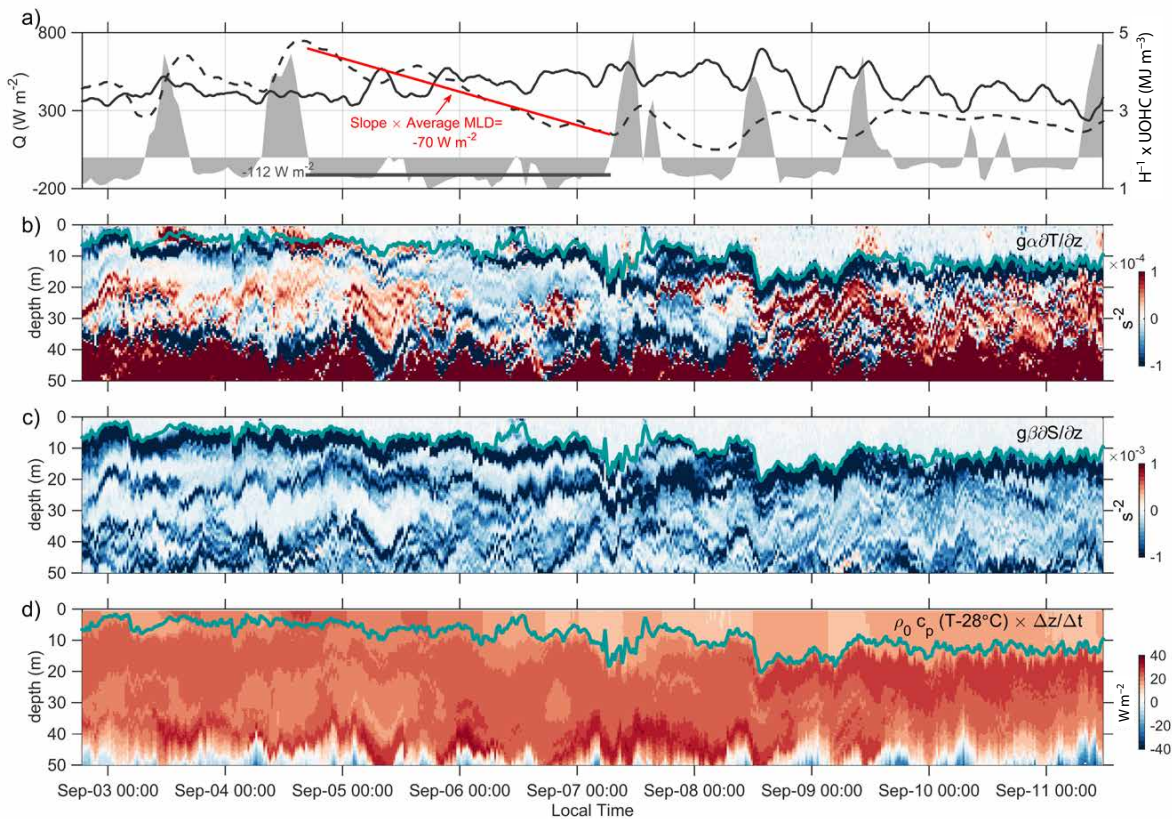


**FIGURE 4.** Time series from  $\chi\text{SOLO-N}$  showing the (a) net surface heat flux (shading, left-hand side) and average upper-ocean heat content below (black solid line, right-hand side) and above (black dashed line, right-hand side) the mixed layer, (b) contribution of temperature to density stratification, (c) contribution of salinity to density stratification, and (d) upper-ocean heating relative to  $28^\circ\text{C}$  converted to a rate using a time scale of one day. Mixed layer depth (turquoise line), calculated as the depth at which the density exceeds  $0.03 \text{ kg m}^{-3}$  of the value at  $0.5 \text{ m}$ , is plotted in (b–d). Note color axes differ by a factor of 10 in (b) and (c).

## DEVELOPMENT OF THE DIURNAL WARM LAYER

The development of the DWL is detailed for both floats on September 3–4 (Figure 5) when  $\chi$ SOLO-S was near 16.6°N, 89.2°E and  $\chi$ SOLO-N was near 17.3°N, 89.4°E (i.e., a separation of roughly 80 km north-south). Prior to sunrise, the isothermal layer was deeper than 10 m at the southern float and shallower than 10 m at the northern float (Figure 5b,c). For both floats, the temperature increased with depth at this time, indicative of the subsurface warm layers evident in Figures 2 and 3. After the transition to net heating at the surface (around 0930 IST), the temperature at 0.5 m begins to increase. As the day progresses, warming occurs preferentially near the surface due to the exponential decrease in penetrating shortwave radiation. Temperature within the DWL is greater than in the previous evening's isothermal layer, resulting in depth curves that are characterized by the development of a minimum in temperature near 5–10 m depth. Later in the day, near-surface mixing acts to homogenize the DWL, creating a sharply peaked minimum at the base of the DWL (intermediate shades in Figure 5b,c). As time progresses, the

sharpness of the temperature minimum is eroded via mixing. Cooling at the surface further reduces elevated near-surface temperature, and eventually a well-mixed region overlying a subsurface warm layer again characterizes temperature profiles.

The daily evolution of the vertical derivative of temperature,  $\partial T/\partial z$  within and at the base of the DWL follows a repeatable pattern, characterized by alternating bands of positive and negative  $\partial T/\partial z$  (Figures 2e and 3e). As the DWL develops, relatively warm water resides above relatively cool water. At night, after the temperature stratification of the DWL is eroded, relatively cool water resides above relatively warm water. The alternating sign of  $\partial T/\partial z$  is a direct consequence of both strong insolation, which provides the heat necessary to form the temperature stratification within the DWL, and strong salinity stratification, which inhibits mixing beneath the mixed layer and supports subsurface maxima in temperature. During the day, temperature within the DWL rivals or exceeds that in the subsurface maxima. At night, the well-mixed and cool surface layer is directly in contact with subsurface warm layers. The daily fluctuation in the sign of the

temperature gradient determines the sign of the turbulent heat fluxes within the upper ocean, as discussed below.

## TURBULENT HEAT FLUX IN THE DIURNAL WARM LAYER

$\chi$ SOLO floats were equipped with  $\chi$ Pods that measure temperature and temperature gradient fluctuations at 100 Hz using FP07 thermistors (Moum and Nash, 2009; Perlin and Moum, 2012). The resultant frequency spectra are converted to wavenumber spectra using the ascent rate of the  $\chi$ SOLO floats ( $\sim 0.2 \text{ m s}^{-1}$ ) and scaled to theoretical spectra to estimate the diffusive rate of destruction of temperature gradient variance ( $\chi$ ). A turbulent diffusivity of temperature ( $K_T$ ) is computed directly as  $K_T = \frac{1}{2} \chi \{\partial T/\partial z\}^{-2}$ . The turbulent heat flux is calculated as  $J_q^h = -\rho_0 c_p K_T \partial T/\partial z$ .

The highest values of  $K_T$  ( $\geq 10^{-3} \text{ m}^2 \text{ s}^{-1}$ ) are contained within the surface mixed layer (Figures 2f and 3f). In contrast, diffusivity is very weak below the mixed layer, with median diffusivity near  $10^{-6} \text{ m}^2 \text{ s}^{-1}$  in both float records. Apart from the distinction between the surface mixed layer and values at depth, spatial/temporal variability is not pronounced. Sporadically, elevated diffusivity appears in layers along temperature-salinity features (e.g., just below 20 m depth on days 6 and 7 in the  $\chi$ SOLO-S record), but these events are not obviously linked to tidal or wind forcing over these short records. The near-surface mixing is reduced at the outcropping of the salinity front on day 4 in the  $\chi$ SOLO-S record, but otherwise it remains elevated throughout the record.

$J_q^h$  alternates sign within the mixed layer on a daily basis, reflecting the sign of the temperature gradient within the DWL. At night, relatively cool water resides above relatively warm water, and upper-ocean turbulence acts to warm SST. Once the DWL has developed, relatively warm water resides above relatively cool water, and subsurface turbulence acts to cool SST. On days with strong insolation, this daily cycle can be seen as regions of alternating positive

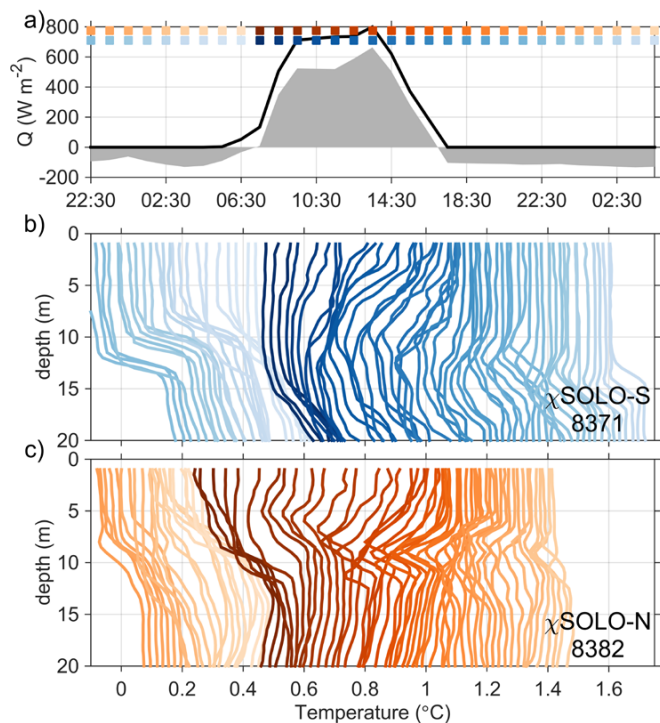


**FIGURE 5.** (a) Net surface heating (shading) and insolation (black line). Upper-ocean temperature evolution as measured on September 4, 2015, for (b)  $\chi$ SOLO-S and (c)  $\chi$ SOLO-N. Temperature profiles are referenced to the mean of the first profile in the upper 20 m, and subsequent profiles are offset by  $0.02^{\circ}\text{C}$ . Color of profiles indicates time of day with darkest shades denote the transition to positive net heat flux. Colored squares in (a) are spaced evenly every hour so that profile times in (b) and (c) may be appropriately referenced.

and negative heat fluxes within the mixed layer (Figures 2g and 3g). The magnitude of the heat flux within the upper 10 m is roughly  $10\text{--}20\text{ W m}^{-2}$ , fluctuating around zero along with the net surface heat flux (although the precise phasing is complicated, Figures 2a and 3a). Subsurface mixing, therefore, acts to damp the diurnal SST cycle—cooling during the day when surface fluxes warm and warming at night when surface fluxes cool. This response depends on stable, salinity-controlled mixed layers, which cap the depth of the DWL and support subsurface storage of heat.

Below the DWL, mixing was weak, and  $J_q^h$  was indistinct from zero to below 40 m depth. This depth region marked the location where temperature decreased below  $28^\circ\text{C}$  and the lower limit in the summation for UOHC. If these mixing values are representative of longer time series (e.g., those presented in Warner et al., 2016, in this issue), heat exported beneath the mixed layer is efficiently stored in the upper ocean and available for tapping by strong surface forcing, for example, during the passage of a tropical cyclone. Low mixing is also consistent with the strong layering observed in the float records. When surface layers are capped by new freshwater, for example, through lateral spread of riverine input, the remnant mixed layer is effectively decoupled from the surface. Weak mixing slowly erodes the pre-existing stratification at the base of the remnant mixed layer, creating the potential for multiple temperature inversions and layers of enhanced salinity stratification to develop over time.

### THE IMPORTANCE OF NEAR-SURFACE SALINITY STRATIFICATION

Even though a DWL developed on every day with net heating, its character varied due to surface conditions (winds and heat flux) and the initial stratification. Sensitivity to these conditions is demonstrated by comparison of DWL heating on two days with similar surface heat flux but differing winds and stratification.

Time series shown in Figure 6 compare the DWL development in weakly stratified, moderate wind conditions (salinity varies by 0.5 psu over the upper 25 m with wind stress close to  $0.2\text{ N m}^{-2}$ ) to strongly stratified, low-wind conditions (salinity varies by 2 psu over the upper 25 m with wind stress close to  $0.1\text{ N m}^{-2}$ ).

On both days, the onset of net surface heating occurred near 0630 IST with peak surface heat flux exceeding  $600\text{ W m}^{-2}$  (Figure 6a,d). Both time series also show subsurface warm layers at daybreak near 15 m depth. The DWL extended much deeper and was less stratified under moderate wind forcing and weak salinity stratification (Figure 6b). Over the upper 7.5 m, temperature varied by only  $0.025^\circ\text{C}$  (Figure 6c) near the peak surface heat flux. By late afternoon (1430 IST), the upper ocean was well mixed for a short period of time prior to surface cooling, resulting

in a weakly unstable temperature gradient. In contrast, temperature stratification was stable in the DWL under weak winds and high salinity stratification (Figure 6e). Immediately after the transition to net surface heating, temperature stratification developed in the upper 7.5 m (Figure 6f). At its peak, the difference in temperature over the upper 7.5 m exceeded  $0.15^\circ\text{C}$ . Temperature within the DWL became well mixed slightly later in the day (relative to the net heat flux cycle) compared to the moderate wind case, after which the temperature gradient reversed weakly (i.e., slightly cooler water resides above warmer water in the upper 7.5 m).

For similar surface forcing, the maximum temperature in the DWL will depend on the pre-existing salinity stratification. The float data show that the amplitude of the temperature cycle in the DWL ( $\Delta T$ , calculated as the maximum temperature

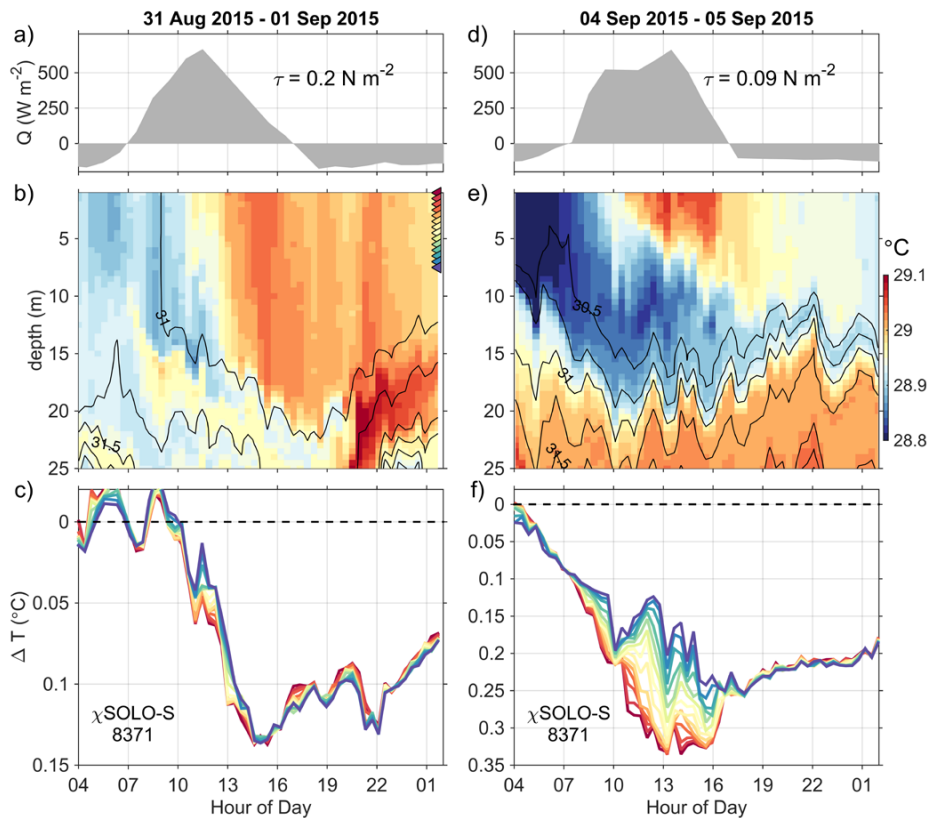


**FIGURE 6.** Comparison of diurnal warm layer development on days with similar net surface heat flux (a,d) but with low (a–c) and high (d–f) salinity stratification. (b,e) Temperature (color shading) and salinity (contours) from  $\chi$ SOLO-S. (c,f) Diurnal warm layer evolution shown as the difference between upper-ocean temperature and SST at the start of the time series. Line color indicates depth of time series records with respective positions marked on the right-hand side of (b). Note different temperature limits in (c) and (f). Average wind stress over the shown time series is given in (a) and (d).

difference over 24 hours at 0.5 m depth) is correlated with the upper ocean stratification ( $N^2 = g\rho_0^{-1} \partial\rho/\partial z$ , calculated as the daily maximum depth-mean stratification over the upper 25 m). Weaker stratification is associated with a smaller  $\Delta T$ , and stronger stratification is associated with a larger  $\Delta T$  (Figure 7). Although the magnitude of  $\Delta T$  will depend on other factors, (e.g., values with low daily mean surface heating reside below the correlation line), these data show the importance of the initial ocean state to DWL development. Shallow near-surface fresh layers can trap heat over a small vertical expanse, creating larger oscillations in the daily SST cycle.

This overall response competes with the damping of the daily SST cycle by turbulent heat flux. Given the relative magnitudes of the turbulent heat flux compared to the net surface heat flux, we expect that the depth of the DWL, which depends on the magnitude of the salinity stratification, will be the more significant contributor to the overall amplitude of SST in the DWL. This argument is consistent with the significant correlation shown in Figure 7. However, we note that the strength of the subsurface warm layers (and therefore the magnitude of the temperature gradient at the base of the mixed layer) does not scale directly with the upper-ocean salinity

stratification. Although cooling by turbulent fluxes during the day depends on temperature stratification within the DWL (and hence depends on the net surface heat flux and salinity stratification), warming by subsurface mixing at night is relatively independent of the daily heating cycle. Consequently, damping by turbulent fluxes does not solely depend on the vertical scale of the DWL (e.g., compare warming at night during the first few days of the  $\chi$ SOLO-S record, Figure 2a, to the first few days of the  $\chi$ SOLO-N record, Figure 3a), and these competing effects can act independently of one another.

### SUMMARY

Understanding the coupling between the atmosphere and the ocean is critical for improved monsoon prediction (Fu et al., 2003; Inness and Slingo, 2003; Bernie et al., 2005). A serious obstacle to addressing this challenge is that the complexity of BoB upper-ocean stratification has yet to be reasonably represented within regional models (Vinayachandran and Nanjundiah, 2009). Interplay between upper-ocean salinity stratification and temperature stratification creates the potential for a rich and varied response in turbulent heat fluxes and SST, thus impacting air-sea exchange. These relatively short time series from

the southwest monsoon demonstrate three fundamental effects of upper-ocean structure on heat exchange within the ocean-atmosphere system.

First, turbulent mixing of heat below the mixed layer is very low ( $<1 \text{ W m}^{-2}$ ) because it is effectively isolated from surface forcing by strong salinity stratification at the base of the mixed layer. Over most of the upper 50 m, the ocean is warm, with temperature in excess of  $28^\circ\text{C}$ , a common threshold for atmospheric convection. Once this heat is isolated from the mixed layer (e.g., through capping by fresh riverine water), it is effectively stored for later use, since vertical redistribution by subsurface mixing is weak. This heat represents a potentially important energy source during the cyclone season and the transition to the northeast monsoon.

Second, the stabilizing influence of salinity stratification supports the existence of subsurface warm layers. Subsurface warm layers and stratification within the DWL combine to produce alternating signs of the upper-ocean temperature gradient on a daily basis. During the day, relatively warm water in the DWL overlies relatively cool water; at night, relatively cool surface water overlies the subsurface warm layer. The turbulent heat flux within the mixed layer fluctuates about zero along with the alternating sign of the temperature gradient. Turbulence mixes relatively cool water toward the surface during the day, and relatively warm water toward the surface at night. The net result is that subsurface mixing acts to damp the daily SST cycle in the DWL—cooling during the day and warming at night.

Finally, these data show a direct correlation between the intensity of near-surface salinity stratification and the magnitude of the daily SST cycle within the DWL. Although the magnitude of the daily SST cycle will depend on several factors (e.g., the net cumulative heat flux, albedo, optical transmission, and winds), overall shallow fresh layers can trap heat near the surface causing a larger amplitude daily SST cycle. This dependence is

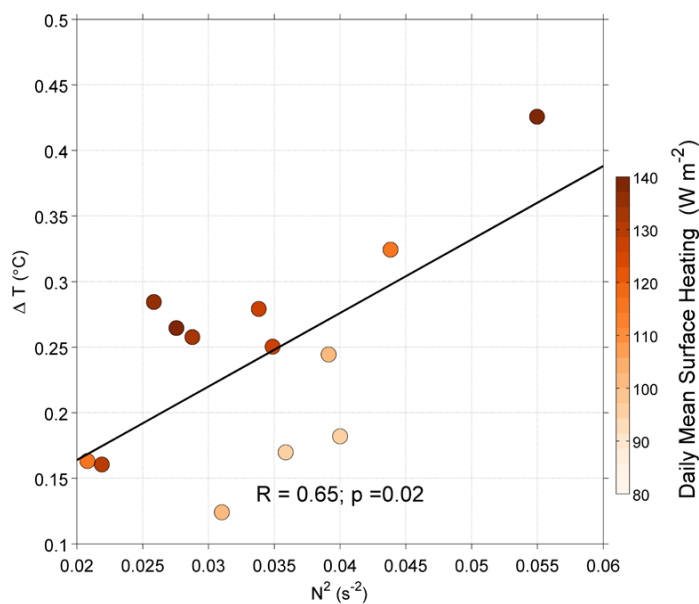


**FIGURE 7.** Maximum daily sea surface temperature oscillation versus peak stratification in the upper 25 m. Shading indicates the cumulative positive net surface heat flux. Only days when the daily mean surface heating exceeds  $60 \text{ W m}^{-2}$  are considered. This criterion is equivalent to considering days when the maximum net heat flux exceeded  $250 \text{ W m}^{-2}$ .

in competition with damping of the SST cycle by turbulent entrainment.

Even at the diurnal time scale, feedbacks between the ocean and the atmosphere influence longer-term variability, including intraseasonal oscillations (Bernie et al., 2005; Woolnough et al., 2007; Guemas et al., 2011; Mujumdar et al., 2011). More generally, appropriately resolving the upper-ocean salinity and temperature structure is needed for improved representation of air-sea interactions in forecast models. These data highlight the complexity of the upper-ocean structure in the BoB even within the upper few meters of the ocean, and demonstrate the value in measurement platforms that can provide well-resolved, clean near-surface data. 

## REFERENCES

- Agarwal, N., R. Sharma, A. Parekh, S. Basu, A. Sarkar, and V.K. Agarwal. 2012. Argo observations of barrier layer in the tropical Indian Ocean. *Advances in Space Research* 50:642–654, <http://dx.doi.org/10.1016/j.asr.2012.05.021>.
- Bernie, D.J., S.J. Woolnough, J.M. Slingo, and E. Guilyardi. 2005. Modeling diurnal and intraseasonal variability of the ocean mixed layer. *Journal of Climate* 18:1,190–1,202, <http://dx.doi.org/10.1175/JCLI3319.1>.
- Fairall, C.W., E.F. Bradley, J.S. Godfrey, G.A. Wick, J.B. Edson, and G.S. Young. 1996. Cool-skin and warm-layer effects on sea surface temperature. *Journal of Geophysical Research* 101:1,295–1,308, <http://dx.doi.org/10.1029/95JC03190>.
- Fu, X., B. Wang, T. Li, and J.P. McCreary. 2003. Coupling between northward-propagating, intraseasonal oscillations and sea surface temperature in the Indian Ocean. *Journal of the Atmospheric Sciences* 60:1,733–1,753, [http://dx.doi.org/10.1175/1520-0469\(2003\)060<1733:CBNIOA>2.0.CO;2](http://dx.doi.org/10.1175/1520-0469(2003)060<1733:CBNIOA>2.0.CO;2).
- Gadgil, S., P. Joseph, and N.V. Joshi. 1984. Ocean-atmosphere coupling over monsoon regions. *Nature* 312:141–143, <http://dx.doi.org/10.1038/312141a0>.
- Goswami, B., M. Wheeler, J. Gottschalck, and D. Waliser. 2011. Intraseasonal variability and forecasting: A review of recent research. Pp. 389–407 in *The Global Monsoon System: Research and Forecast*, 2<sup>nd</sup> ed. [http://dx.doi.org/10.1142/9789814343411\\_0023](http://dx.doi.org/10.1142/9789814343411_0023).
- Goswami, B.N., G. Wu, and T. Yasunari. 2006. The annual cycle, intraseasonal oscillations, and road-block to seasonal predictability of the Asian summer monsoon. *Journal of Climate* 19:5,078–5,099, <http://dx.doi.org/10.1175/JCLI3901.1>.
- Goswami, B.N., S.A. Rao, D. Sengupta, and S. Chakravorty. 2016. Monsoons to mixing in the Bay of Bengal: Multiscale air-sea interactions and monsoon predictability. *Oceanography* 29(2):18–27, <http://dx.doi.org/10.5670/oceanog.2016.35>.
- Guemas, V., D. Salas-Méila, M. Kageyama, H. Giordani, and A. Voldoire. 2011. Impact of the ocean mixed layer diurnal variations on the intraseasonal variability of sea surface temperatures in the Atlantic Ocean. *Journal of Climate* 24:2,889–2,914, <http://dx.doi.org/10.1175/2010JCLI3660.1>.
- Inness, P.M., and J.M. Slingo. 2003. Simulation of the Madden-Julian Oscillation in a coupled general circulation model: Part I. Comparison with observations and an atmosphere-only GCM. *Journal of Climate* 16:345–364, [http://dx.doi.org/10.1175/1520-0442\(2003\)016<0345:SOTMJO>2.0.CO;2](http://dx.doi.org/10.1175/1520-0442(2003)016<0345:SOTMJO>2.0.CO;2).
- Johnson, N.C., and S.-P. Xie. 2010. Changes in the sea surface temperature threshold for tropical convection. *Nature Geoscience* 3:842–845, <http://dx.doi.org/10.1038/ngeo1008>.
- Kalnay, E., M. Kanamitsu, R. Kistler, W. Collins, D. Deaven, L. Gandin, M. Iredell, S. Saha, G. White, and J. Woollen. 1996. The NCEP/NCAR 40-year reanalysis project. *Bulletin of the American Meteorological Society* 77:437–471, [http://dx.doi.org/10.1175/1520-0477\(1996\)077<0437:TNYRP>2.0.CO;2](http://dx.doi.org/10.1175/1520-0477(1996)077<0437:TNYRP>2.0.CO;2).
- Lukas, R., and E. Lindstrom. 1991. The mixed layer of the western equatorial Pacific Ocean. *Journal of Geophysical Research* 96(S01):3,343–3,357, <http://dx.doi.org/10.1029/90JC01951>.
- McPhaden, M.J., and G.R. Foltz. 2013. Intraseasonal variations in the surface layer heat balance of the central equatorial Indian Ocean: The importance of zonal advection and vertical mixing. *Geophysical Research Letters* 40:2,737–2,741, <http://dx.doi.org/10.1002/grl.50536>.
- Mignot, J., C. De Boyer Montégut, and M. Tomczak. 2009. On the porosity of barrier layers. *Ocean Science* 5:379–387, <http://dx.doi.org/10.5194/os-5-379-2009>.
- Moum, J.N. 2015. Ocean speed and turbulence measurements using pitot-static tubes on moorings. *Journal of Atmospheric and Oceanic Technology* 32:1,400–1,413, <http://dx.doi.org/10.1175/JTECH-D-14-00158.1>.
- Moum, J.N., and J.D. Nash. 2009. Mixing measurements on an equatorial ocean mooring. *Journal of Atmospheric and Oceanic Technology* 26:317–336, <http://dx.doi.org/10.1175/2008JTECHO6171>.
- Mujumdar, M., K. Salunke, S.A. Rao, M. Ravichandran, and B.N. Goswami. 2011. Diurnal cycle induced amplification of sea surface temperature intraseasonal oscillations over the Bay of Bengal in summer monsoon season. *IEEE Geoscience and Remote Sensing Letters* 8:206–210, <http://dx.doi.org/10.1109/LGRS.2010.2060183>.
- Perlin, A., and J.N. Moum. 2012. Comparison of thermal variance dissipation rates from moored and profiling instruments at the equator. *Journal of Atmospheric and Oceanic Technology* 29:1,347–1,362, <http://dx.doi.org/10.1175/JTECH-D-12-00019.1>.
- Rao, R.R., and R. Sivakumar. 2003. Seasonal variability of sea surface salinity and salt budget of the mixed layer of the north Indian Ocean. *Journal of Geophysical Research* 108(C1), 3009, <http://dx.doi.org/10.1029/2001JC000907>.
- Roemmich, D., S. Riser, R. Davis, and Y. Desaubies. 2004. Autonomous profiling floats: Workhorse for broad-scale ocean observations. *Marine Technology Society Journal* 38:21–29, <http://dx.doi.org/10.4031/0025533204787522802>.
- Schott, F.A., and J.P. McCreary. 2001. The monsoon circulation of the Indian Ocean. *Progress in Oceanography* 51:1–123, [http://dx.doi.org/10.1016/S0079-6611\(01\)00083-0](http://dx.doi.org/10.1016/S0079-6611(01)00083-0).
- Sengupta, D., G.N. Bharath Raj, and S.S.C. Shenoi. 2006. Surface freshwater from Bay of Bengal runoff and Indonesian Throughflow in the tropical Indian Ocean. *Geophysical Research Letters* 33, L22609, <http://dx.doi.org/10.1029/2006GL027573>.
- Sengupta, D., B.N. Goswami, and R. Senan. 2001. Coherent intraseasonal oscillations of ocean and atmosphere during the Asian summer monsoon. *Geophysical Research Letters* 28:4,127–4,130, <http://dx.doi.org/10.1029/2001GL013587>.
- Smyth, W.D., and J.N. Moum. 2001. Three-dimensional (3D) turbulence. Pp. 2,947–2,955 in *Encyclopedia of Ocean Sciences*. J.H. Steele, ed., Academic Press, Oxford, UK, <http://dx.doi.org/10.1006/rwos.2001.0134>.
- Sobel, A.H., E.D. Maloney, G. Bellon, and D.M. Frierson. 2008. The role of surface heat fluxes in tropical intraseasonal oscillations. *Nature Geoscience* 1:653–657, <http://dx.doi.org/10.1038/ngeo312>.
- Vinayachandran, P.N., and R.S. Nanjundiah. 2009. Indian Ocean sea surface salinity variations in a coupled model. *Climate Dynamics* 33:245–263, <http://dx.doi.org/10.1007/s00382-008-0511-6>.
- Warner, S.J., J. Becherer, K. Pujiana, E.L. Shroyer, M. Ravichandran, V.P. Thangaprakash, and J.N. Moum. 2016. Monsoon mixing cycles in the Bay of Bengal: A year-long subsurface mixing record. *Oceanography* 29(2):158–169, <http://dx.doi.org/10.5670/oceanog.2016.48>.
- Weller, R.A., J.T. Farrar, J. Buckley, S. Mathew, R. Venkatesan, J. Sree Lekha, D. Chaudhuri, N. Suresh Kumar, and B. Praveen Kumar. 2016. Air-sea interaction in the Bay of Bengal. *Oceanography* 29(2):28–37, <http://dx.doi.org/10.5670/oceanog.2016.36>.
- Woolnough, S.J., F. Vitart, and M.A. Balmaseda. 2007. The role of the ocean in the Madden-Julian Oscillation: Implications for MJO prediction. *Quarterly Journal of the Royal Meteorological Society* 133:117–128, <http://dx.doi.org/10.1002/qj.4>.

## ACKNOWLEDGMENTS

We thank Captain Chris Curl and the crew of R/V *Revelle* for their help with the field operations. Engineering of the  $\chi$ SOLO floats involved the expertise of Pavan Vutukur, Mike Neeley-Brown, and Craig Van Appledorn at Oregon State University and Michael McClune and Chris Berg from the Instrument Development Group at Scripps Institution of Oceanography. Meteorological data comes from the 18°N WHOI mooring supported by the Upper Ocean Processes Group (R. Weller). R. Venkatesan's group at the National Institute of Ocean Technology, Chennai, India, on ORV *Sagar Nidhi*, helped support mooring deployment and recovery. This work was funded by Office of Naval Research grants N00014-14-1-0236 (ELS, JNM), N00014-13-1-0483 (DLR), N00014-13-1-0453 (JTF), and N00014-12-1-0938 (SKV, AG).

## AUTHORS

**Emily L. Shroyer** (eshroyer@coas.oregonstate.edu) is Assistant Professor, College of Earth, Ocean, and Atmospheric Sciences, Oregon State University, Corvallis, OR, USA. **Daniel L. Rudnick** is Professor, Scripps Institution of Oceanography, University of California San Diego, La Jolla, CA, USA. **J. Thomas Farrar** is Associate Scientist, Woods Hole Oceanographic Institution, Woods Hole, MA, USA. **Bungho Lim** is Faculty Research Assistant, College of Earth, Ocean, and Atmospheric Sciences, Oregon State University, Corvallis, OR, USA. **S. Karan Venayagamoorthy** is Associate Professor, Department of Civil and Environmental Engineering, Colorado State University, Fort Collins, CO, USA. **Louis C. St. Laurent** is Associate Scientist, Woods Hole Oceanographic Institution, Woods Hole, MA, USA. **Amrapalli Garanaik** is a graduate student in the Department of Civil and Environmental Engineering, Colorado State University, Fort Collins, CO, USA. **James N. Moum** is Professor, College of Earth, Ocean, and Atmospheric Sciences, Oregon State University, Corvallis, OR, USA.

## ARTICLE CITATION

Shroyer, E.L., D.L. Rudnick, J.T. Farrar, B. Lim, S.K. Venayagamoorthy, L.C. St. Laurent, A. Garanaik, and J.N. Moum. 2016. Modification of upper-ocean temperature structure by subsurface mixing in the presence of strong salinity stratification. *Oceanography* 29(2):62–71, <http://dx.doi.org/10.5670/oceanog.2016.39>.